PLEASE CITE THIS ARTICLE AS DOI: 10.1063/5.0153513

Accepted to Phys. Fluids 10.1063/5.0153513

Face Masks Provide High Outward Protection Despite Peripheral Leakage: Insights from a Reduced-Order Model of Face Mask Aerodynamics

Chuanxin Ni (倪传鑫), 1 Tomas Solano, 2 Kourosh Shoele, 2 Jung-Hee Seo (서정희), 1 and Rajat Mittal (रजत मित्तल)*1,3

1) Department of Mechanical Engineering, Johns Hopkins University, Baltimore, Maryland 21218,

USA

2) Department of Mechanical Engineering, Florida A&M University-Florida State University, Tallahassee, Florida 32307,

³⁾Department of Medicine, Johns Hopkins School of Medicine, Baltimore, Maryland 21205,

(*Author to whom correspondence should be addressed: mittal@jhu.edu)

(Dated: 2 June 2023)

A reduced-order model of face mask aerodynamics and aerosol filtration is introduced. This model incorporates existing empirical data on filtration efficiency for different types of face masks, as well as the size distribution of exhaled aerosol particles. By considering realistic peripheral gap profiles, our model estimates both the extent of peripheral leakage and the fitted filtration efficiency of face masks in terms of outward protection. Simulations employing realistic peripheral gap profiles reveal that for surgical masks, 80% or more of the total exhaled airflow could leak through the mask periphery, even when the average peripheral gap measures only 0.65 mm. However, the majority of exhaled aerosol particles do not follow the flow path through the peripheral gaps, but instead, impact directly on the mask fabric. As a result, these face masks can filter out approximately 70% of the exhaled particles despite the significant peripheral leakage. To validate our model, we compare its predictions with experimental data, and we find a reasonable agreement in estimating the outward protection provided by surgical masks. This validation underscores the reliability of our model in assessing the efficacy of surgical masks. Moreover, leveraging the insights gained from our model, we explore the impact of mask usage on the transmission of respiratory viruses within communities. By considering various scenarios, we can assess the potential reduction in viral spread achieved through widespread mask adoption.

I. INTRODUCTION

Face masks emerged as a simple yet important tool for helping contain the spread of the SARS-CoV-2 virus during the COVID-19 pandemic, and the coming years have observed continued usage of face masks among the public as well as in healthcare settings 1-5. Several studies have shown that face mask usage among the public is an effective strategy to mitigate transmission of pathogens that are responsible for a variety of respiratory illnesses such as the common cold, influenza, COVID-19, and others^{4,6-8}. Proper selection and usage of a face mask, however, remains a challenge due to the complex factors that can impact the effectiveness of face masks⁹. This effectiveness is a function of the fabric/material used in the mask, the peripheral gaps due to the mask-face fit, the aerosol particle sizes in consideration, and the flow features associated with the particular respiratory activity (breathing, coughing, sneezing, etc.) being considered. The cost and ease of use are also important factors for the public to select a mask which may be worn over extended periods of time. Tools that can quantify and assess the effectiveness of face masks would be quite useful not only in the selection of appropriate face masks. but also in designing more effective face masks.

A. Airborne Transmission of Respiratory Viruses

The airborne transmission of viruses such as SARS-CoV-2 and influenza occurs when virus-laden respiratory aerosol particles exhaled by an infected person during activities such

as coughing, sneezing, talking and even breathing, are inhaled by a susceptible person. The aerosol particles that contribute to this mode of transmission have a size smaller than about 5 µm; they can suspend in the air for hours and can be entrained into the inhalation current of a person^{10,11}. This airborne transmission route plays an essential role in the rapid spread of respiratory diseases like COVID-19 and is hard to detect and prevent ^{12,13}. Thus, the key outward protective function of a face mask is to filter out as many of these particles before they are released into the ambient air surrounding the infected

While sneezing and coughing are generally associated with the generation of large quantities of expelled aerosol particles, and the spread of respiratory viruses is generally attributed to these expiratory events, SARS-CoV-2 is unique in this respect since infected people can emit virus-laden aerosol particles *before* the appearance of symptoms such as sneezing and coughing ¹². Thus, expulsion of aerosol particles during breathing has played an important role in the COVID-19 pandemic¹⁴. Consequently, understanding and quantifying the ability of face masks to trap the exhaled particles during normal breathing is particularly important, and this forms the motivation of the current study.

B. Outward Fitted Filtration Efficiency (oFFE) of Face Masks

When particles penetrate the fabric of a mask, they are collected by the fabric via several mechanisms: particle diffusion, particle-fiber interception, impaction, and electrostatic depo-

sition caused by a charge difference⁹. Many recent studies have provided evidence that face mask usage among the public has been effective in reducing the transmission and spread of the SARS-CoV-2 virus^{4,6}. Quantifying the effectiveness of a face mask, however, continues to be a challenge primarily due to the inevitable peripheral leakage⁹. Moreover, as mentioned in Mittal, Ni, and Seo¹², this leakage is typically larger during exhalation (outward protection) than inhalation (inward protection), which becomes a bigger issue for the outward protection of face masks. Hui *et al.*¹⁵ investigated the exhaled flow behaviors associated with coughing with and without masks and found that none of the commonly worn masks (e.g., N95, surgical and cloth masks) can entirely prevent the peripheral leakage. Other studies that have visualized the peripheral leakage and the jets emanating from the peripheral gaps 16-18 found that all tested masks experience leakage during normal breathing, especially from the top edge of the masks. The studies also stated that both the mask fabric and the mask-face fit play a critical role in determining the face mask effectiveness. Particularly interesting results were described by Drewnick et al. 17 for homemade face masks; they found that a leakage with a total area between 0.5% and 2% of the mask area is typical, and this leads to a decline in the mask filtration efficiency (FE) to a value between 50% and 67%.

Nevertheless, most certification standards of face masks only require manufacturers to test and provide the minimum filtration efficiency (FE_{min}) at the most penetrating particle size (MPPS) as a representation of the mask performance without taking account of the peripheral leakage and the respiratory activities 19-21. This testing regime is driven primarily by the fact that most face masks are certified for protection against environmental pollutants, and therefore the focus is almost exclusively on the inward protection. Moreover, FE measurements of different mask fabrics can vary widely according to different references²¹⁻²³, which creates additional uncertainty in using this metric. Therefore, it is improper to solely use the fabric FE to represent the face mask effectiveness. Fitted filtration efficiency (FFE) is a better alternative metric used to quantify the filtration efficiency of masks when worn (or fitted on the face) by a person²⁴, but most of relevant studies are focused on inward protection offered by face masks, not the outward protection we are interested in. In the current study, we estimate the outward fitted filtration efficiency (oFFE) of face masks using a model that includes key factors such as the FE variance against different particle diameters D, the peripheral leakage and the aerosol particle adherence to airflow. Detailed modeling of oFFE will be discussed in Section II.

C. Modeling Human Exhalation with Face Masks

Computational modeling of human respiration with a face mask has the potential to quantify the face mask effectiveness without carrying out experiments for each face mask and maskface combination. Several previous studies have attempted to establish fully resolved three-dimensional computational fluid dynamic (CFD) models of face masks. Lei et al. 25 synthesized a finite-element CFD model to examine the peripheral

leakage locations and strength between different head forms and an N95 mask and showed that leakage usually occurs at the nose (40%) and the cheeks (26% on each side). A computational model of human respiration with a face mask developed by Dbouk and Drikakis²⁶ employed a multiphase CFD model in a fully coupled Eulerian-Lagrangian framework. Dbouk and Drikakis²⁶ suggested that the criteria used to evaluate the face mask effectiveness should be modified to incorporate the effects from droplet penetration and the fluid dynamics of mask peripheral leakage. More recently, Solano et al.27 have demonstrated the capabilities of a new computational model that simulates the deployment of face masks on a variety of synthesized faces, which was combined with a particle dispersion model to predict the effectiveness of face masks.

Despite continued efforts to model the human respiration with a face mask⁹, a simple and effective reduced-order face mask model considering the peripheral leakage, different mask fabrics, and various mask-face combinations is missing. Unlike the above fully resolved three-dimensional face mask model, reduced-order computational models have the advantage of rapidly performing thousands of simulations with various face masks and mask-face combinations. Such models could serve as a rapid designing and analyzing tool for the face mask industry as well as for certification organizations.

The objectives of the current study are to: (a) develop a reduced-order computational model of face mask aerodynamics during exhalation, taking into account both the peripheral leakage and varying mask fabrics/materials, (b) examine the combined effect of peripheral gap sizes and mask fabric properties on the peripheral leakage, and (c) predict the outward fitted filtration efficiency (oFFE) of a large variety of face masks that are typically worn by the public.

II. MATERIALS AND METHODS

A. Evaluation of Outward Fitted Filtration Efficiency (oFFE)

In Fig. 1, we present a schematic of aerosol particle dynamics and flow behaviors during human exhalation with a face mask. The effectiveness of face masks is commonly quantified by measuring the filtration efficiency (FE) over a relevant range of particle diameters (D) without any peripheral leakage. Within the context of the schematic in Fig. 1, $FE(D) = N_F/(N_F + N_P)$, and FE is a strong function of the particle diameter D. The minimum value of this filtration efficiency (FE_{min}), which usually occurs for diameters D of about 0.3 µm, is often used as the single parameter to define the effectiveness of a face mask. For instance, various public health organizations and regulatory agencies around the world have set definitions and standards for the performance of face masks^{19–21}. While these might differ in specific details, overall, there are three main face mask categories: fitted facepiece (FFP) masks (which includes N95 masks), surgical or medical procedure masks, and cloth masks. FFP masks are further categorized into FFP1, FFP2, and FFP3 masks based on their $FE_{min},$ and the FE_{min} of them are prescribed as 80%, 94%, and 99%, respectively.

PLEASE CITE THIS ARTICLE AS DOI: 10.1063/5.0153513

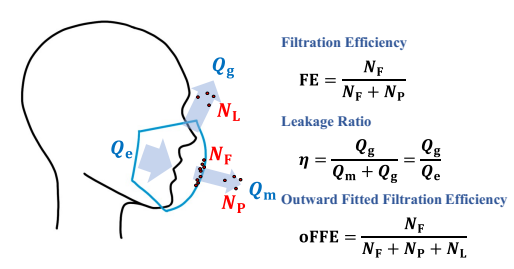


FIG. 1: Schematic of aerosol particle dynamics and critical parameters: a schematic of aerosol particle dynamics is presented for human exhalation with a face mask. Beside it are critical parameters that are related to the oFFE evaluation. $N_{\rm F}$, $N_{\rm P}$, and $N_{\rm L}$ are the number of particles filtered by the mask fabric, penetrating through the mask fabric, and leaking via the peripheral gaps, respectively. $Q_{\rm e}, Q_{\rm m}$, and $Q_{\rm g}$ are the volume flow rates of exhalation, mask penetration, and peripheral leakage, respectively. η represents the leakage ratio defined by the flow rates, and oFFE is the outward fitted filtration efficiency.

However, FEmin at MPPS is a poor indicator of the actual face mask effectiveness since firstly, it underestimates the net filtration of aerosol particles by the face mask over the range of particle diameters relevant to airborne transmission (which ranges from 0.1 to about 10 µm), and secondly, it does not account for the peripheral leakage (see Mittal, Breuer and Seo9, and references therein). This has motivated the introduction of outward fitted filtration efficiency (oFFE), a metric which corresponds to the outward filtration efficiency of a face mask when it is worn by a person^{28,29}. The key difference between FE and oFFE is due to the aerosol particles that leak through the gaps that appear between the periphery of the mask and the face when the mask is worn by a person^{30,31}. With reference to the schematic in Fig. 1, oFFE = $N_F/(N_F + N_P + N_L)$. However, as pointed out by Mittal. Breuer, and Seo⁹, estimation of this particle leakage N_L is highly nontrivial since it depends not only on the filtration efficiency of the mask fabric but also on the leakage ratio given by $\eta = Q_g/Q_e$, where Q_e is the total volume flow rate from the nose (or mouth) during exhalation and Q_g is the volume flow rate through the peripheral gaps. This leakage ratio itself depends on the mask type, the maskface fit and the total volume flow rate Q_e , i.e.,

$$\eta = \eta(\text{mask}, \text{fit}, Q_e).$$
(1)

If we suppose that the leakage ratio is available via simulations or experiments, a simple but naive estimation of oFFE would be obtained by assuming that all the aerosol particles follow the airflow and therefore the particle leakage ratio $N_L/(N_F+N_P+N_L)$ (different from oFFE) is exactly equal to the leakage ratio η defined by the volume flow rates. With this assumption, oFFE = FE(1 – η). However, as pointed out by Mittal, Breuer, and Seo 9 , only the small particles are expected to follow the airflow, and respiratory aerosol, especially during exhalation, could contain large droplets that will not follow

the airflow. Thus, the above estimation of oFFE should be adjusted to account for the fraction of particles that do not adhere to the airflow.

Following Mittal, Breuer, and Seo⁹, the dependency of oFFE on the aerosol particle adherence to airflow is modeled via the introduction of an airflow adherence ratio σ , which represents the fraction of particles that adhere to the airflow. This parameter is expected to be a function of the particle Stokes number given by Stk = $\rho_p DU/18\mu$, where ρ_p is the density of particle, U is the exhaled flow velocity at the nose or mouth, and μ is the air dynamic viscosity. Assuming that the number of exhaled aerosol particles are proportional to the flow rate Q_a , we can separate the exhaled particles into a fraction proportional to σQ_e that follow the airflow and a fraction $(1 - \sigma)Q_e$ that do not (see Fig. 2). Among the particles that follow the airflow, a fraction proportional to $\eta \sigma Q_e$ will escape with the peripheral leakage flow, and the remaining, proportional to $(1 - \eta)\sigma Q_e$, will go along with the mask-penetrating flow and be filtered according to the FE of the mask fabric. The large particles expelled from the nose/mouth will not follow the airflow and, given the directivity of the exhaled jet (see Fig. 2), their inertia will carry them towards the mask fabric. These particles that have a total number proportional to $(1-\sigma)Q_e$ will also be filtered by the mask according to the FE of the fabric. Thus, the probability $(P_{\rm F})$ of a particle of diameter D being filtered by the mask is equal to

$$P_{F}(D, \text{mask, fit}) = FE(D) \times \sigma(\text{Stk}) \times (1 - \eta)$$

$$+ FE(D) \times [1 - \sigma(\text{Stk})] \qquad (2)$$

$$= FE(D) [1 - \sigma(\text{Stk})\eta].$$

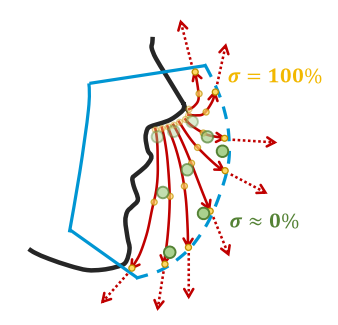


FIG. 2: Schematic of exhaled airflow from nose and particle behaviors based on airflow adherence ratio σ : yellow (small) particles with $\sigma=100\%$ adhere to the airflow, whereas green (large) particles with $\sigma\approx0\%$ do not.

Given that the exhaled aerosol contains particles with a range of diameters, the oFFE for a given distribution of particle diameters can then be estimated as

offE =
$$\begin{split} & \int_{D_0}^{D_1} P_{\rm F}(D) P_{\rm E}(D) {\rm d}D \\ & = \int_{D_0}^{D_1} {\rm FE}(D) \left[1 - \sigma({\rm Stk}) \eta \right] P_{\rm E}(D) {\rm d}D, \end{split} \tag{3}$$

PLEASE CITE THIS ARTICLE AS DOI: 10.1063/5.0153513

Accepted to Phys. Fluids 10.1063/5.0153513

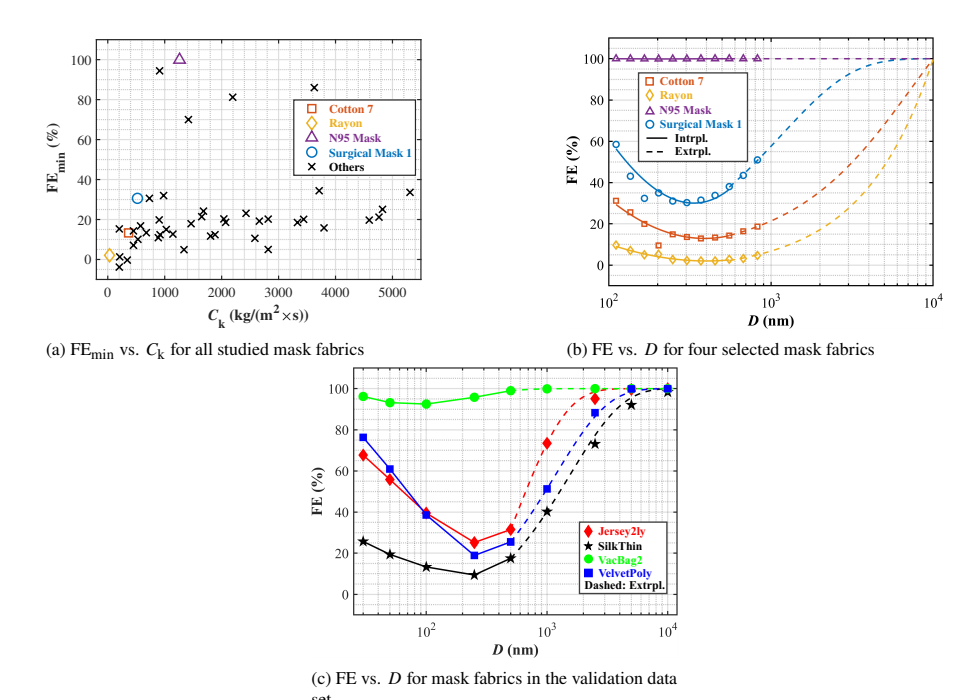


FIG. 3: Measured FE_{min} and constructed FE(D) functions for mask fabrics: (a) Experimental data of FE_{min} at MPPS are adopted from Zangmeister $et~al.^{32}$ for all studied mask fabrics. The x-axis is the fabric air resistance C_k . Four fabrics are highlighted by different markers in the figure, which will be used as examples for the constructed FE(D) functions in (b). The fabric names and corresponding markers are displayed in the legend. The names for the fabrics in this study are consistent with those used in Zangmeister $et~al.^{32}$ unless otherwise stated; (b) Constructed FE(D) functions from 0.1 to 10 µm are shown for four selected mask fabrics. The colored markers represent the measured FE of the fabrics covering from 111 to 825 nm, and the solid and dashed curves display the FE interpolation and extrapolation results by regression covering from 111 to 553 nm and from 553 nm to 10µm, respectively. The selected fabrics are also reported in the legend; (c) Validation of the FE extrapolating method presented in (b) is shown here. The same method is now applied to the experimental FE data set in Drewnick $et~al.^{17}$ covering from 30 nm to 10 µm and measured at a flow velocity of 12.9 cm/s. Exponential functions are fitted to the FE data points at D=250,500 nm and then extended to 10 µm where FE is set to 100%. The markers in the figure represent the measured FE data. The solid curves connect the experimental data from 30 nm to 500 nm, while the dashed curves depict the extrapolated FE functions from 500 nm to 10 µm. Fabric names shown in the legend are consistent with those used in Drewnick $et~al.^{17}$, each of which has been assigned a distinct marker shape and color. For more details about the validation, readers are referred to the Supplementary Sec. S-I.

where $P_{\rm E}(D)$ is the probability density function (PDF) of aerosol particle diameter associated with the particular exhalation event under consideration (breathing, sneezing, coughing, etc.), and D_0 and D_1 are the lower and upper limits of relevant particle diameter, respectively. Thus, determination of the oFFE for a mask for outward protection during breathing requires estimates of FE(D), η (mask, fit, $Q_{\rm e}$), σ (Stk), and $P_{\rm E}(D)$. The following subsections address each of these estimates.

B. Face Mask Filtration Efficiency (FE)

The expression for oFFE in Eq. 3 requires FE as a function of particle diameter D and for this, we employ the comprehensive experimental FE data from Zangmeister $et\,al.$ ³² for various mask fabrics. The FE_{min} data at the MPPS of all the fabrics are presented against C_k in Fig. 3a, where C_k is the corresponding air resistance of each fabric, the definition and details of which will be discussed in Sec. II C 1. As depicted in the figure, for a single FE_{min} value around 20%, extremely large variation

4

PLEASE CITE THIS ARTICLE AS DOI: 10.1063/5.0153513

Studies have demonstrated that exhaled aerosol particles that carry the pathogens predominantly consist of small particles $(D < 5 \, \mu \mathrm{m})^{10.11}$, and the largest D of particles that can suspend in still air for 5 seconds and be inhaled by a person within a 1 to 2-meter distance from the emitter is $100 \, \mu \mathrm{m}^{11}$. In light of this, the lower and upper limits for particle diameter in the present study, denoted as D_0 and D_1 , are set at $100 \, \mathrm{nm}$ and $10 \, \mu \mathrm{m}$, respectively, where the lower limit corresponds to the size of SARS-CoV-2 virus³⁴ and the upper limit is a typical maximum diameter generated under normal breathing conditions³⁵.

The measurements of Zangmeister $et~al.^{32}$, however, do not extend particle diameters beyond 825 nm. To construct FE(D) functions from D_0 to D_1 , we therefore use regression to interpolate the FE data within the measured range from 100 to 553 nm and extrapolate for larger particle diameters from 553 nm to 10 μ m. The interpolation over the experimental FE data employs rational polynomials as the candidate function, while for the extrapolation, we employ exponential functions which are consistent with established analytical derivations of FE for fibrous media 33 ,36. Since all the face masks in the data set of Zangmeister $et~al.^{32}$ have a pore size smaller than 10 μ m, we set FE at 10 μ m equal to 100%. Fig. 3b displays the constructed FE(D) functions for four selected mask fabrics and the interpolations provide fits with $\overline{R^2} > 0.9$.

Further validation of the FE extrapolating method has been carried out by applying the same exponential function to a different data set 17 which contains experimentally measured FE data up to D=10 µm but only for a few mask fabrics. Fig. 3c shows the validation results for the FE data of four fabrics measured at an airflow velocity of 12.9 cm/s. Very good agreements ($\overline{R^2}>0.9$) are observed between the extrapolated dashed curves and experimental data, which convinces us that the extrapolation method proposed can substantially capture the FE variation at large particle diameters and provide reasonable estimation of FE values. More details of this validation process are included in Supplementary Sec. S-I. Furthermore, the shape of the constructed functions displayed in Fig. 3b and 3c follows the general pattern of the FE(D) functions of fibrous media shown in the references 32,36,37 . These functional fits to the FE are used in the evaluation of oFFE later.

C. Peripheral Leakage Ratio (η)

Determination of the peripheral leakage from a mask involves two elements: (a) quantification of the gap sizes around the periphery of a mask, and (b) a method to compute the flow rates from the gaps given a mask and the profile of the peripheral gap sizes. Both elements are described in this section.

1. Aerodynamic Models for Exhaled Flow with Face Masks and Peripheral Gaps

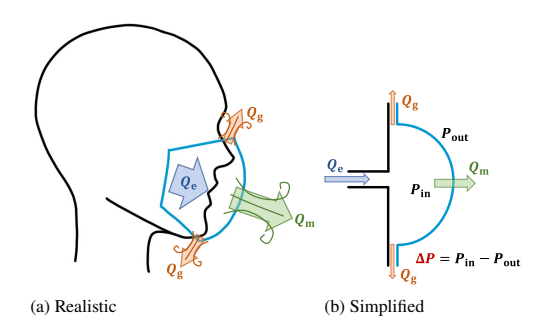


FIG. 4: Schematic of human exhalation with a face mask

The physical process of exhalation is depicted schematically in Fig. 4. The exhaled flow coming out of the nose and/or mouth impinges on the face mask. Some of this flow penetrates the mask fabric, while the rest leaks from the peripheral gaps. In Fig. 4a and 4b, Q_e is the exhaled volume flow rate, and $Q_{\rm m}$ and $Q_{\rm g}$ represent the flow rates penetrating the mask fabric and leaking through the peripheral gaps, respectively. ΔP measures the pressure difference across the face mask from inside (P_{in}) to outside (P_{out}) . These symbols will be used consistently throughout this paper. The current reduced-order model is inspired by the model of Perić and Perić³⁸ and is schematically shown in Fig. 4b. In the current model, exhalation associated with breathing is modeled as a time-invariant flow, and therefore, the details of the flow inside the mask are mostly neglected to simplify the modeling process. We note that this assumption is reasonable for breathing, but might not be so for highly transitory exhaled activities such as coughing and sneezing. For those activities, due to the high exhaling velocity up to about 10 m/s³⁹, the Reynolds number of the flow can reach around $O(10^4)$, resulting in a more complex flow inside the mask. As a result, the pressure could also have large spatial variation inside the mask and around the mask periphery. These factors could therefore result in highly unexpected flow behaviors that cannot be substantially captured by the model shown in Fig. 4b because it has already neglected the flow details inside the mask. Furthermore, with such a high flow velocity, the movement of the face mask caused by the exhaling jet cannot be ignored¹². This movement could lead to significant changes in the peripheral gap sizes and thus

PLEASE CITE THIS ARTICLE AS DOI: 10.1063/5.0153513

in the prediction of peripheral leakage. However, in the current model, the face masks are assumed to be static. Thus, extension of the current model for events such as coughing and sneezing is not simple. In the present study, we will focus on the breathing activity, since infected people of COVID-19 could emit virus-laden aerosol particles before the appearance of obvious symptoms.

Fabrics used for face masks are usually made of natural or synthetic fibers which are overlaid together, either in an organized manner or in a random weave, to form mask fabric layers³². These fabric layers can be regarded as a porous medium, and the aerodynamic model for such a medium is generally formulated via the Darcy-Forchheimer law^{23,33,40}. Specifically, in the current model, the relationship between the pressure difference across the mask fabric ($\Delta P_{\rm m}$) and the average through-flow velocity (\overline{u}_m) should be modeled by Darcy-Forchheimer law, which considers the linear (Darcy's law) and quadratic (Forchheimer's law) dependency of $\Delta P_{\rm m}$ on $\overline{u}_{\rm m}$. Based on the measurements of previous studies 39,41,42 , the through-flow velocity \overline{u}_{m} for exhalation is expected to be in the range from about 1 m/s to 5 m/s. Moreover, the average pore sizes for a reusable cloth mask, a surgical mask, and an N95 mask are around 47, 33, and 30 µm, respectively 43. Combining with the air properties at 20°C, the Reynolds number of the airflow penetrating the mask fabric is estimated to O(10)for all the studied fabrics, so the penetrating airflow could be considered as laminar flow. Therefore, the linear effect of $\overline{u}_{\rm m}$ is expected to be dominant, and the relationship between $\Delta P_{\rm m}$ and \overline{u}_{m} can therefore be adequately described by Darcy's law as follows:

$$\Delta P_{\rm m} = C_{\rm k} \overline{u}_{\rm m} = C_{\rm k} \frac{Q_{\rm m}}{A_{\rm m}},\tag{4}$$

where C_k is the air resistance of the fabric and A_m is the fabric filtering area. For the current study, $A_{\rm m}$ is chosen to be 319.35 cm2, which is a typical value used for medium-sized face masks⁴⁴. To cover a range of representative face masks, the comprehensive data set from Zangmeister et al. 32 with data for 45 mask fabrics is used in the current study. The air resistance C_k of each fabric can be derived based on the measurements of $\Delta P_{\rm m}$ and $\overline{u}_{\rm m}$ in Zangmeister et al.³², and further details about the experiments and fabric properties can be found in Supplementary Sec. S-II.

Direct aerodynamic modeling of the entire face mask gaps along the periphery with variable gap sizes can be a complicated task. Instead, we follow Perić and Perić³⁸ in assuming a gap segment with a narrow width along the mask periphery for modeling the peripheral gap flow. This narrow gap segment is assumed to be in the shape of a rectangular channel which has a uniform length (L_g) , width (B_g) , and height (or gap size, H_g). Following Perić and Perić³⁸, the pressure loss through this narrow gap segment can be modeled as a combination of a major loss through the bulk of the channel (ΔP_c) and a minor loss associated with the entrance and exit (ΔP_{ee}):

$$\Delta P_{g} = \Delta P_{c} + \Delta P_{ee}$$

$$= \frac{12\mu L_{g}\overline{u}_{c}}{H_{g}^{2}} + (\zeta_{in} + \zeta_{out})\frac{1}{2}\rho\overline{u}_{c}^{2},$$
(5)

where \overline{u}_c is the cross-sectional average leakage velocity, and $\zeta_{\rm in}$ and $\zeta_{\rm out}$ are the loss coefficients for the entrance and exit with values of 0.5 and 1.0, respectively³⁸. Furthermore, μ is the air dynamic viscosity at 20° C with a value of 1.813×10^{-5} Pa·s, and ρ is the air density at 20°C with a value of 1.204 kg/m³. L_g is fixed at 1.0 cm according to Perić and Perić³⁸. The low Reynolds number of the flow through the narrow gap segment due to a maximum gap size not exceeding 5 mm provides some justification for assuming a two-dimensional channel flow profile inside the gap segment. Coupled with the expression $\overline{u}_c = Q_g/B_gH_g$, the final expression for the pressure drop across the gap segment is as follows:

$$\Delta P_{\rm g} = \frac{12\mu L_{\rm g}Q_{\rm g}}{B_{\rm g}H_{\rm g}^3} + (\zeta_{\rm in} + \zeta_{\rm out})\frac{1}{2}\rho \frac{Q_{\rm g}^2}{\left(B_{\rm g}H_{\rm g}\right)^2}.$$
 (6)

2. Realistic Peripheral Gap Profiles

Perić and Perić 38 proceeded with their modeling by assuming a uniform gap size H_g along the mask periphery. However, it is well known that the gap size varies significantly along the periphery and Fig. 5a shows the results from Solano, Mittal, and Shoele44 where the gap size variation was computed via simulations of a quasi-static mechanical model without any exhaling flow. Large gaps appeared at both sides of the nose, at the center of cheeks, and at the lower portion of the face mask. This is also borne out by other studies 18,27,45,46 as well as by personal experience. Indeed, for the case shown in Fig. 5b, while the average gap size is about 1 mm, local gap sizes can exceed 5 mm. Given the highly non-linear dependence of the pressure drop ΔP_g on the gap size H_g (see Eq. 6), a model that accounts for the large variation in gap size along the periphery should provide higher accuracy. Thus, instead of using a uniform gap size $H_{\rm g}$ in the face mask aerodynamic model like Perić and Perić³⁸, in the current model, we augment the reduced-order model to account for the realistic peripheral gap profile that appears along the mask periphery.

To obtain the spatial variation of the peripheral gaps, the quasi-static mechanical model from Solano, Mittal, and Shoele⁴⁴ was applied, and rectangular face masks (a typical shape for surgical and cloth face masks) were deployed onto representative face forms without any exhaling flow. To reach the final position of the masks on the face forms, the elastic bands were first elongated and wrapped around the ears. The length of the bands then decreased gradually during the deploying process until it reached the final values, pulling the masks onto the face forms. The minimum energy concept was utilized to determine the equilibrium locations of discretized points on the masks at every intermediate deployment stage between the initial and final mask positions. This method takes into account the total elastic energy from the mask fabric, the mask periphery, and the ear bands, as well as the contact force between the mask and the face tissues. For more details, readers are referred to the original paper by Solano, Mittal, and Shoele⁴⁴. Fig. 5e displays a schematic of the mask deployment. Four types of gap profile are used in the current study and presented in Fig. 5a, 5b, 5c, and 5d, which correspond

PLEASE CITE THIS ARTICLE AS DOI: 10.1063/5.0153513

Accepted to Phys. Fluids 10.1063/5.0153513

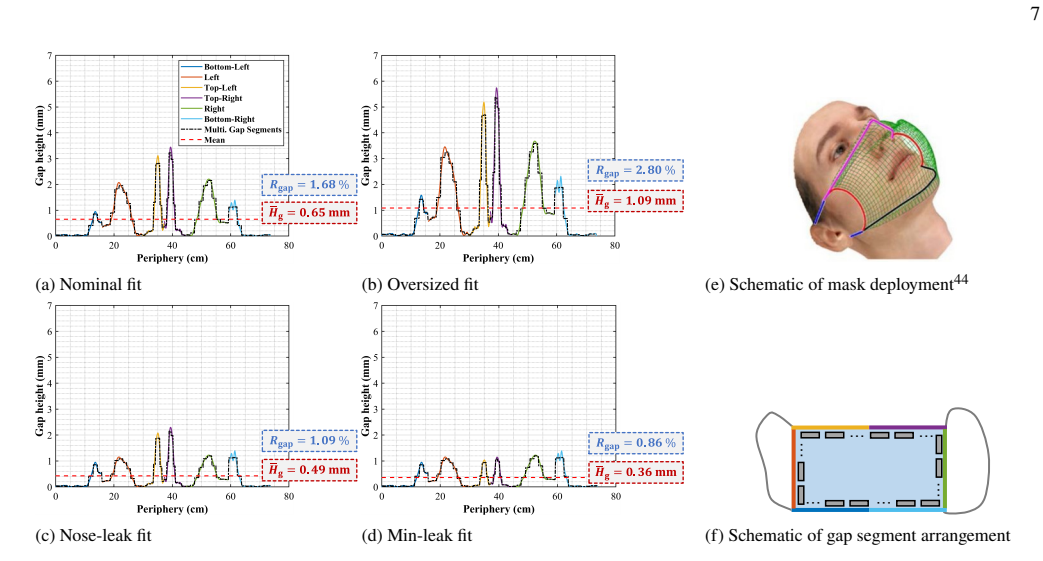


FIG. 5: **Realistic peripheral gap profiles:** profiles are obtained from the quasi-static mechanical model⁴⁴, which represents typical mask-face fits. These profiles are approximated by utilizing multiple narrow gap segments along the periphery; (a), (b), (c), and (d): Realistic peripheral gap profiles for four typical mask-face fits. The average gap size \overline{H}_g and the gap area ratio R_{gap} are also shown in the figures; (e): An example of how the quasi-static mechanical model obtains the gap profiles; (f): This schematic illustrates how the narrow gap segments are arranged along the mask periphery to approximate the realistic gap profiles. The rectangles along the mask periphery stand for the narrow gap segments.

to the following typical mask-face fits respectively: (a) nominal fit, (b) oversized fit, (c) nose-leak fit, and (d) min-leak fit. In Fig. 5a, 5b, 5c, and 5d, the solid-colored curves represent the gap sizes along the periphery, which are obtained directly from the mechanical model. The dashed black curves in these figures show the approximated gap profiles which are achieved by arranging multiple narrow gap segments along the periphery. The arrangement of the gap segments and how the approximated profiles are achieved will be explained in detail in the subsection following this one. The average gap size $\overline{H}_{\rm g}$ and the gap area ratio $R_{\rm gap}$ of each profile are also reported in these figures. $\overline{H}_{\rm g}$ is evaluated by averaging the gap sizes along the periphery for each profile, while $R_{\rm gap}$ is calculated by dividing the total peripheral gap area over the total mask area $A_{\rm m}$.

The nominal fit profile in Fig. 5a represents the fit where a typical face mask is deployed reasonably onto a face. The average gap size $\overline{H}_{\rm g}$ for this case is 0.65 mm and the gap area ratio $R_{\rm gap}$ is 1.7%. The other three gap profiles in Fig. 5b, 5c, and 5d are generated by modifying this profile. The oversized fit profile represents the condition when the fit of a mask on a face is loose, and $\overline{H}_{\rm g}$ is increased to an average of 1.09 mm. The nose-leak fit profile is meant to model the situation of face mask usage when a reasonably well-fitted surgical mask is used^{44,47} but with a large gap near the nose. An $\overline{H}_{\rm g}$ of 0.49 mm is achieved for this case. Finally, the min-leak fit profile corresponds to the circumstance of a mask with a very good

fit to a face, where \overline{H}_g is only 0.36 mm.

3. Lumped-Element Model for Peripheral Leakage Ratio (η)

As mentioned in the previous subsection, the gap size (or height) variation in the presented profiles in Fig. 5 is captured by segmenting the gaps along the periphery into n narrow gap segments (see Fig. 5f), each of which has a height $(H_{g,i}, i=1,\ldots,n)$ corresponding to the value in the profiles at the location of current segment along the mask periphery. In the current study, a total of 60 narrow gap segments (n=60) are utilized to cover the entire periphery (the periphery has a total length of 73.70 cm), which leads to a segment width B_g of approximately 1.23 cm. As can be seen from Fig. 5a, 5b, 5c, and 5d, the approximated profiles by using 60 narrow gap segments provide a reasonable representation of the spatially varying gap profiles. The lumped-element reduced-order model for face mask aerodynamics can then be developed by assembling all the components into the equivalent circuit shown in Fig. 6.

In the equivalent circuit in Fig. 6, the exhaled volume flow rate $Q_{\rm e}$ is divided into the branch currents $Q_{\rm m}$ and $Q_{\rm g,i}$, i=1,...,n that represent the flow rates penetrating the mask fabric and leaking through each narrow gap segment, respectively. In the current study, the exhaled flow rate $Q_{\rm c}$ is set to 30 L/min, which is a typical value of adults' breathing during

PLEASE CITE THIS ARTICLE AS DOI: 10.1063/5.0153513

Accepted to Phys. Fluids 10.1063/5.0153513

FIG. 6: Lumped-element equivalent circuit: the current in the circuit represents the volume flow rate, and the voltage stands for the pressure difference. The mask fabric and the narrow gap segments on the periphery are modeled as the parallel resistors which share the same pressure difference ΔP across the face mask.

light activities 48,49 . Due to the assumption of uniform pressure inside the mask, the pressure difference across the mask fabric and through each narrow gap segment is assumed to be the same, namely $\Delta P = \Delta P_{\rm m} = \Delta P_{\rm g,i}$, so a parallel resistor design is adopted in the equivalent circuit. The air resistance of the mask fabric and the narrow gap segments are modeled by the resistors $R_{\rm m}$ and $R_{\rm g,i}$, i=1,...,n, and the values of these resistors can be calculated by dividing the pressure difference over the corresponding flow rates. The system of equations for this lumped-element model can therefore be written in the final form as:

$$\Delta P = C_k \frac{Q_{\rm m}}{A_{\rm m}},\tag{7a}$$

$$\Delta P = \frac{12\mu L_{\rm g} Q_{\rm g,i}}{B_{\rm g} H_{\rm g,i}^3} + (\zeta_{\rm in} + \zeta_{\rm out}) \frac{1}{2} \rho \frac{Q_{\rm g,i}^2}{\left(B_{\rm g} H_{\rm g,i}\right)^2}, i = 1, ..., n,$$
(7b)

$$Q_{\rm e} = Q_{\rm m} + \sum_{i=1}^{n} Q_{\rm g,i}.$$
 (7c)

By solving Eq. 7 together, the mask-penetration flow rate $Q_{\rm m}$ and the leakage flow rate $Q_{{\rm g},i}$ through each gap segment can be obtained, and these flow rate data are then used for estimating the leakage ratio η with its dependence on different mask fabrics embedded in the value of $C_{\rm k}$, and on the mask-face fits via $H_{{\rm g},i},i=1,...,n$.

D. airflow Adherence Ratio (σ)

The airflow adherence ratio σ , which describes the proportion of aerosol particles that adhere to the airflow, is a function of the particle Stokes number. By definition, the particle Stokes number is the ratio of the particle relaxation time over the flow characteristic time, and it quantifies the extent to which a particle is driven by its own inertia. To provide closure to the current model and to evaluate oFFE by Eq. 3, the dependence of the airflow adherence ratio σ on the Stokes number needs to be established.

Fig. 2 shows a schematic of the path of exhaled flow and aerosol particles inside the mask. The flow streams out of the

nostrils towards the mask, and then make a turn (often more than 90 degrees) as it moves towards and escapes through the peripheral gaps. An estimate of σ is needed for this turning flow condition. Several experiments and models have estimated the particle deposition efficiency (DE; ratio of the deposited particles over the total particles) for turning flows. For instance, Cheng and Wang 50 and Pui, Romay-Novas, and Liu 51 have measured the deposition of particles in a pipe flow undergoing a 90-degree bend and have shown a smooth and monotonic variation in DE from 0% deposition at Stk =0 to >90% deposition at Stk ≈1 (see Fig. 7). We note that in the context of the current model, $\sigma(\text{Stk})=1-\text{DE}(\text{Stk}),$ and we can therefore use these data to estimate the airflow adherence ratio $\sigma(\text{Stk}).$

8

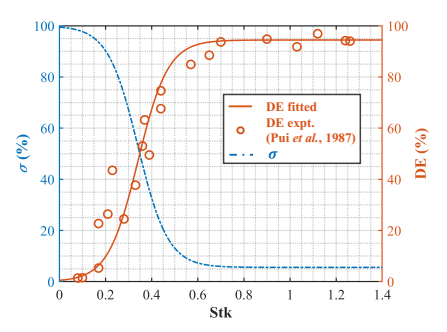


FIG. 7: Particle deposition efficiency (DE) and airflow adherence ratio (σ (Stk)): experimental DE data (right y-axis) for a 90-degree turning flow 51 with Reynolds number of 1000 and the sigmoid function (hyperbolic tangent) fitted to them (right y-axis) are plotted against particle Stokes number Stk. Airflow adherence ratio σ (left y-axis) derived from DE is also presented here as a dash-dotted curve. The two y-axes are shown in percentage for understanding convenience.

The particular data that is employed here is for a flow Reynolds number of 1000, which corresponds reasonably well to the exhaled flow from the nostrils given a flow rate of 30 L/min, a typical nostril area^{52,53} of 330 mm², and an average jet velocity of 1.5 m/s. To compute the particle Stokes number (Stk = $\rho_p DU/18\mu$), the air dynamic viscosity μ of 1.813×10^{-5} Pa·s corresponding to a temperature of 20°C is also used here, and the particle density $\rho_{\rm p}$ is chosen to be the same as that of water (ρ_p =1000 kg/m³). In Fig. 7, the orange circles represent the experimental DE data from Pui, Romay-Novas, and Liu⁵¹, and the orange solid curve is a sigmoid function fitted to the data. As can be seen from the figure, the fitted curve provides a reasonable fit to the experimental data, with an R-square value of around 0.96. One important observation from the figure is that, as the particle diameter goes up and the Stk rises above 1, the DE does not asymptotically approach 100% but rather fluctuates around 95%. A possible reason for this is that when impacting on the solid surface, these large particles might rebound from the surface or break up into smaller particles, reducing the detected DE values⁵¹.

PLEASE CITE THIS ARTICLE AS DOI: 10.1063/5.0153513

This feature is well captured by the fitted DE function, and will be considered by the calculation of oFFE (Eq. 3) through the σ function as shown below:

$$\sigma(Stk) = 1 - DE(Stk)$$

$$= 1 - DE_0 - DE_0 \tanh (C_{\sigma} (Stk^* - Stk_c)),$$
(8)

where C_{σ} and Stk_c are the fitting coefficients which have the values of 2.90 and -0.49, respectively. DE_0 is the magnitude of the sigmoid function and has a value of 0.47. Stk values are normalized to Stk^* by the mean and standard deviation of Stk in the experimental data set^{51} ($Stk^* = (Stk - 0.53)/0.38$). The derived $\sigma(Stk)$ function is also shown in Fig. 7 as a dash-dotted curve

We note in closing current discussion that a 90-degree turning pipe flow in Pui, Romay-Novas, and Liu 51 may not be a perfect mimic of the breathing flow impinging onto a face mask. However, in the absence of direct measurements of particle deposition efficiency for a jet impinging onto a surface with a Reynolds number comparable to the current case and for a range of particle sizes, the currently utilized data serve to capture the core mechanisms of particle deposition on a solid surface within a turning flow of Re = 1000, and can be used as a reasonable foundation for estimating the airflow adherence ratio, σ .

E. Aerosol Particle Size Distribution ($P_{\rm E}(D)$) during Exhalation

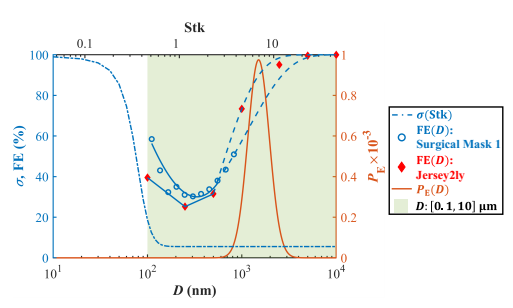


FIG. 8: Airflow adherence ratio ($\sigma(\text{Stk})$), filtration efficiency of selected mask fabrics (FE(D)), and breathing aerosol particle PDF ($P_{\rm E}(D)$): the left y-axis is related to the airflow adherence ratio $\sigma(\text{Stk})$ (dash-dotted line) and filtration efficiency FE(D) (solid and dashed lines), while the right y-axis is the PDF $P_{\rm E}(D)$ (solid line) that corresponds to the normal breathing condition. $\sigma(\text{Stk})$ here is the same as that in Fig. 7, and FE(D) for two selected mask fabrics are adopted from Fig. 3b and 3c. The light green region stands for the relevant diameter range for oFFE evaluation (see Sec. II B).

The focus of the current study is on the exhaled flow during normal breathing, and Fig. 8 presents the probability density function (PDF) ($P_{\rm E}(D)$) of the aerosol particle diameters during normal breathing from Johnson *et al.*³⁵. Employing this

 $P_{\rm E}(D)$ within the current model serves as another key factor that distinguishes the normal breathing condition under focus from other exhaling activities such as coughing/sneezing. This is in addition to the differences of flow behaviors discussed in the previous Sec. II C 1. Johnson et al. 35 have found that, unlike the normal breathing condition where particles are generated solely by the bronchiolar fluid film burst mode (B mode), two additional mechanisms called laryngeal or L mode and Oral or O mode have also contributed to the particle generation during activities like coughing/sneezing. Compared to the breathing PDF, the coughing/sneezing PDF not only has a broader size range that includes larger particles, but it also possesses a higher first peak around 1 um and an additional second peak around 100 µm. These differences in the PDFs would bring about the variations in particle behaviors and change our prediction of the number of filtered particles. Therefore, the normal breathing condition can be well distinguished from coughing/sneezing activities by its distinct PDF $P_{\rm E}(D)$ shown in Fig. 8.

We note that the PDF is centered around a particle diameter of 1.5 $\,\mu m$ and more than 90% of the particles are within a diameter range between 0.8 and 3.0 $\,\mu m$. The upper x-axis shows the corresponding particle Stokes number, and we further note that the peak in PDF corresponds to a relatively large particle Stokes number of about 7.0. Also displayed in the plot (via the left y-axis and the dash-dotted curve) is the airflow adherence ratio $\sigma(Stk)$ estimated in the previous section. For most of the particles in the relevant diameter range, it is apparent that the value of $\sigma(Stk)$ is close to 5% because of the relatively high Stokes number. Thus, most of the exhaled particles will not adhere to the airflow, but will impact directly on the mask fabric instead.

The filtration efficiency of Surgical Mask 1 from Zangmeister $et~al.^{32}$, as well as that of the 2-layer jersey cotton fabric from Drewnick $et~al.^{17}$, are also shown in Fig. 8. These were selected as representative fabrics to show the FE(D) functions constructed by the validated extrapolation method in Fig. 3. It can be seen from the figure that, based on the extrapolation, filtration efficiency is not adequately characterized only by the minimum value FE_min at MPPS around 300 nm. Instead, the effective FE should correspond to the range where $P_{\rm E}(D)$ exhibits high values (in this case, a range from 0.8 to 3.0 µm). Moreover, the airflow adherence ability of aerosol particles depicted by σ should also be considered, which leads to the proposed oFFE metric in the current study. More details of oFFE evaluation will be discussed in Sec. III B.

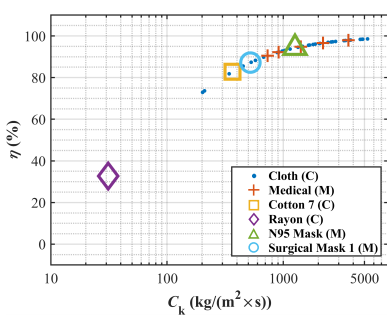
III. RESULTS

Using the models described in Section II, the leakage ratio η and oFFE have been estimated for all the 45 mask fabrics for which FE functions are constructed based on the experimental FE data provided by Zangmeister $et~al.^{32}$. For each mask, we have employed the four distinct peripheral gap profiles to estimate the leakage and analyze the influence on the leakage caused by different profiles. The aerosol particle adherence to airflow has also been considered in the oFFE calculation by

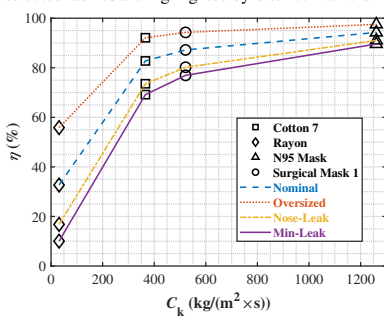
PLEASE CITE THIS ARTICLE AS DOI: 10.1063/5.0153513

utilizing the airflow adherence ratio σ , which is derived from the experimental data from Pui, Romay-Novas, and Liu⁵¹. The particle size distribution ($P_{\rm E}(D)$) chosen here corresponds to a normal breath³⁵, and a validation of oFFE has also been shown in this section by comparing to the experimental data from Pan et al.⁵⁴ and others.

A. Face Mask Peripheral Leakage



(a) Leakage ratio η vs. air resistance C_k for all mask fabrics with the nominal peripheral gap profile: Four selected fabrics are highlighted by distinct markers.



(b) Leakage ratio η vs. air resistance C_k for selected mask fabrics with all realistic peripheral gap profiles

FIG. 9: Leakage ratio η and influence of gap sizes: (a) Leakage ratio defined by the volume flow rates ($\eta = Q_g/Q_e$) for all mask fabrics are plotted against the fabric air resistance C_k . Q_g is the sum of the flow rates of all narrow gap segments, namely $Q_g = \sum_{i=1}^n Q_{g,i}$. Selected fabrics are highlighted here by distinct markers, and their names are listed in the legend. "(C)" and "(M)" appended to the names in the legend denote for cloth and medical-grade fabric categories, respectively. Details of mask fabrics included in each category can be found in Supplementary Sec. S-II; (b) Leakage ratio η of selected mask fabrics are presented for all realistic peripheral gap profiles shown in Fig. 5. Markers for different fabrics and line styles for different profiles are shown in the legend.

The relationship between the peripheral leakage ratio η and fabric air resistance C_k is illustrated in Fig. 9a for all studied mask fabrics under the nominal peripheral gap profile condition. Four selected fabrics are highlighted by distinct markers, and their leakage ratio η variations corresponding to all gap profiles in Fig. 5 are displayed in Fig. 9b. From Fig. 9a, it is obvious that the leakage ratio η increases monotonically with the air resistance C_k when the nominal profile is used and quickly approaches to 100% at around C_k =800 kg/(m²×s). This indicates that even with a face mask like a surgical mask that has a relatively low fabric air resistance $(C_k \approx 550 \text{ kg/(m²×s)})$, the leakage ratio η could go up to 90% easily.

From Fig. 9b, we can observe that the gap size increase increases the peripheral leakage for all selected fabrics. For instance, for the commonly used surgical mask, the leakage flux ranges from 69% for the best fit (min-leak fit), to 93% for the worst fit (oversized fit). Similar to Fig. 9a, for a given gap profile, increased air resistance C_k of the fabric would tend to direct more airflow through the gap and increase peripheral leakage. This is also borne out by the data in the plot where, as C_k increases from O(10) (for the rayon mask) to O(1000) (for the N95 masks), peripheral leakage ratio increases to about 90%. This however leads to a somewhat counter-intuitive situation: for the same mask-face fit, higher quality masks such as the surgical and N95 masks generate larger peripheral leakage than cloth masks. Indeed, for the rayon mask, the leakage flux ranges from about 10% for the worst fit to 56% for the best fit, but for the N95 masks, this range is between 90% and 98%. Thus, even with a good fit where the average gap size is only 0.36 mm, 90% of the exhaled flow is expected to leak from the mask periphery for masks like N95 masks. This might seem to indicate that medical-grade masks would tend to provide a lower oFFE, but as we will show later in Sec. III B, this is not the case.

Peripheral leakage ratio measured by other references via experimental or modeling methods can help us validate the above results. Larsen, Heebøll, and Meyer⁵⁵ carried out inhalation and exhalation experiments with mannequins wearing surgical masks under various volume flow rates. They found that with a 'casual' mask-face fit (which can be considered as the nominal fit in Fig. 5a) and a volume flow rate of 30 L/min, the peripheral leakage ratio can exceed 80%, aligning well with the η results in Fig. 9. Freitag, Howell, and Jim⁵⁶ developed a simple leak model to estimate the reduction of viral load during breathing and speaking as a function of multiple parameters. Results from their model show that the mask (referred to as "Berkshire Mask" in this paper) with an air resistance C_k comparable to the Surgical Mask I in Fig. 9b (C_k =578 kg/(m²×s)) experiences a leakage ratio of over 50%. Considering that this figure was obtained with a lower volume flow rate of 10 L/min and a smaller gap area of 1.57 cm² (smaller than the min-leak fit in Fig. 5d which has a gap area of 2.65 cm2), our leakage ratio results of Surgical Mask I are quite reasonable.

Since the mask periphery is discretized into a series of narrow gap segments, the cross-sectional averaged velocity $\overline{u}_{g,i}$ of each segment can be calculated by dividing the $Q_{g,i}$ obtained from Eq. 7 over the cross-sectional area of the segment, i.e., $B_{g,i} \times H_{g,i}$. This average velocity of all gap segments can

PLEASE CITE THIS ARTICLE AS DOI: 10.1063/5.0153513

then be plotted along the mask periphery to examine the local leakage intensity. Fig. 10 presents the $\overline{u}_{g,i}$ curves of leakage flow velocity along the periphery of Surgical mask 1.

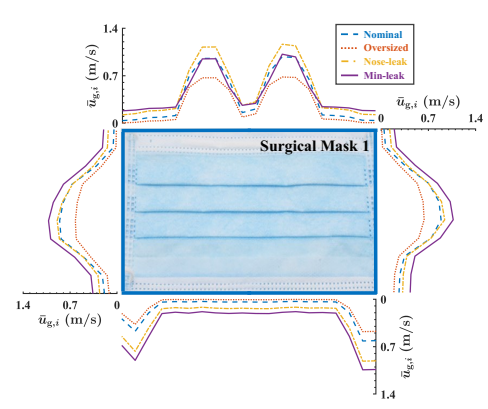


FIG. 10: Leakage velocity along the periphery of Surgical Mask 1: the cross-sectional averaged velocity $\overline{u}_{g,i}$ along the mask periphery are presented for the four gap profiles in Fig. 5. The legend displays the line color and type corresponding to each profile.

For all peripheral gap profiles, the velocity curves indicate large leakage on both sides of the nose, at the center of the side mask edges, and at the corners of the bottom mask edge. These are the periphery regions that have relatively larger gaps (see Fig. 5). As the gap size decreases from the oversized fit to the min-leak fit, the peripheral leakage $Q_{\mathrm{g},i}$ will decrease due to the increase of the gap segment air resistance, which can be derived from Eq. 7b and seen from Fig. 9b. The velocity $\overline{u}_{g,i}$, counter-intuitively, may not decrease with $Q_{g,i}$ but may instead increase due to the reduction of the gap height $H_{g,i}$ and cross-sectional area of each segment. Therefore, to determine $\overline{u}_{g,i}$ at each segment, influences of both $Q_{g,i}$ and $H_{g,i}$ should be considered. Furthermore, we note that the peak velocity magnitudes are in the range of 0.5 to 1.5 m/s, which would result in a Reynolds number of O(100) for the peripheral jet given a gap of O(1 mm). Thus, these leakage jets under a normal breathing condition are expected to be laminar, but higher breathing rates could increase the Reynolds number into transitional and turbulent jet regimes. This quantification of average velocity along the mask periphery has implications for the distance of leakage jets penetration into the surrounding air, as well as the mixing and dispersion of the aerosol particles.

In the three-dimensional flow simulations conducted by Dbouk and Drikakis²⁶, the velocity of leakage flow around the periphery of a surgical mask was quantified. Although their study considered a coughing event with a higher jet velocity of 5.0 m/s and larger peripheral gaps ranging from 4.0 to 14.0 mm, the velocity profile shape around the periphery aligns well with the profile given in Fig. 10 by the current model. Peak velocities are observed on both sides of the nose, at the center of the side mask edges, and at the corners of the

bottom mask edge. Matching the velocity magnitude, however, is challenging with the current model, given that the jet velocity in the present study is 1.5 m/s and the peripheral gaps are, at most, around 6.0 mm. Comparison against the results with Dbouk and Drikakis' three-dimensional simulations²⁶ instills additional confidence that the current lumped-element model is capable of capturing the velocity variation along the mask periphery.

Although only results for Surgical Mask 1 are shown here, similar analyses could be applied to the other mask fabrics included in the current study. For fabrics like Rayon that has relatively lower η , maximum magnitude of the leakage velocity $\overline{u}_{g,i}$ for all peripheral gap profiles would be smaller than 0.4 m/s, and the Reynolds number at the gaps would be around O(30). For masks such as the N95 Mask that has large peripheral leakage, the maximum magnitude of $\overline{u}_{g,i}$ could go up to 1.4 m/s, and the corresponding Reynolds number at the gaps would be around O(100), which is similar to Surgical Mask 1.

B. Outward Fitted Filtration Efficiency (oFFE)

The leakage and mask-through flow rates provide the last piece of data needed to evaluate oFFE for these masks. Results based on the nominal gap profile will be utilized in the subsequent analyses, as it represents the most commonly encountered mask-face fit among the public's mask usage. Fig 11 presents the obtained oFFE results of the mask fabrics in the data set of Zangmeister $et~al.^{32}$. In Fig. 11, the oFFE of each mask is plotted against the peripheral leakage ratio η , the air resistance C_k , and the minimum filtration efficiency FE_{min} at MPPS which were measured by experiments³². Several observations can be made from these plots, and they are enumerated here:

- Despite significant peripheral leakage shown in Fig. 11a (ranging from 85% to nearly 95% of the total flow), all masks with medical-grade fabrics achieve oFFE greater than 70% for outward protection. Fig. 11b reveals the same results more clearly that all the medical-grade fabrics locate at the left-top corner of the plot and outperform most of the cloth fabrics.
- 2. As displayed in Fig. 11a, nearly one-third of the cloth fabric masks can achieve oFFE that exceed 50% with an average leakage ratio (η) over 90%. Several cloth fabrics can even achieve oFFE of around 90% despite η being close to 95%. The same observation could be made from Fig. 11b as well.
- 3. Counter-intuitively, Fig. 11a shows that oFFE generally increases with increasing peripheral leakage ratio, η. Fig. 11b also presents a relatively stronger positive correlation between oFFE and C_k as compared to the correlation between FE_{min} and C_k in Fig. 3a.
- The previous observation can be explained by noting that compared to the FE_{min} measured at the fabric MPPS,

PLEASE CITE THIS ARTICLE AS DOI: 10.1063/5.0153513

Accepted to Phys. Fluids 10.1063/5.0153513

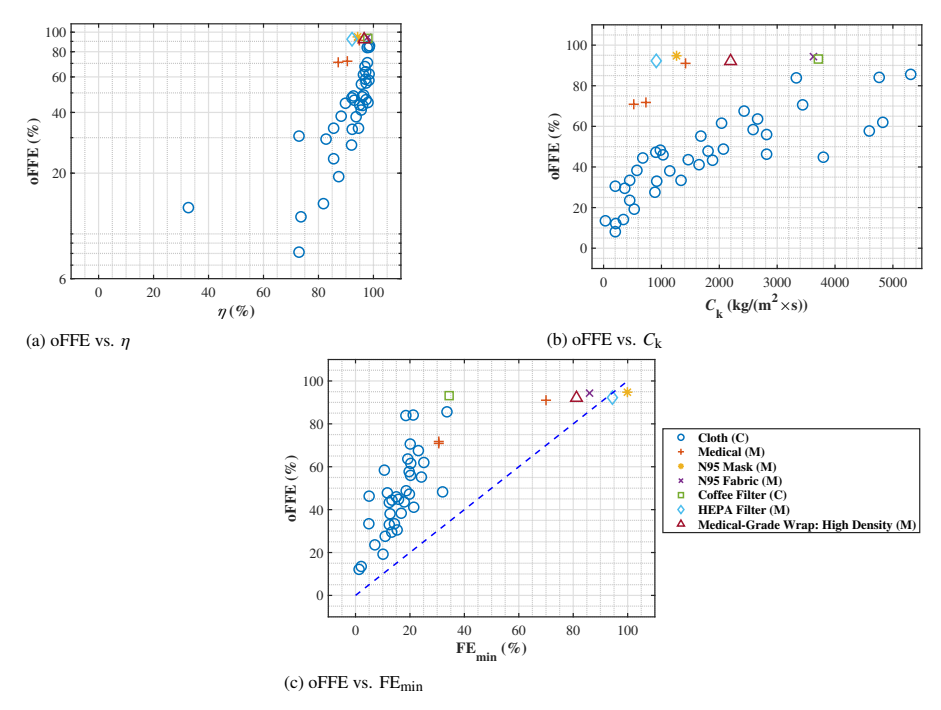


FIG. 11: Outward fitted filtration efficiency (oFFE) of investigated mask fabrics: mask fabrics in Zangmeister et al. 32 are investigated, and their oFFE are presented versus the peripheral leakage ratio η , the air resistance C_k , and the minimum filtration efficiency FE_{min} at MPPS. FE_{min} values of the fabrics are measured by Zangmeister et al. 32 . oFFE for each fabric is evaluated based on Eq. 3 which employs FE, η , σ , and P_E described in Sec. II B, Sec. II C, Sec. II D, and Sec. II E, respectively. The nominal gap profile is applied to obtain η from the lumped-element model in Sec. II C 3. Five fabrics exhibiting the largest five oFFE values are highlighted by different markers, and their names are listed in the legend in (c). The remaining fabrics are classified into the cloth (C) and medical-grade (M) fabric categories, which are also listed in the legend in (c). More details of the fabrics included in each category could be found in Supplementary Sec. S-II. The "(C)" and "(M)" appended to the fabric names in the legend are used to denote the cloth and medical-grade categories, respectively. The blue dashed lines in (c) are the 45 degree line for comparing convenience.

the oFFE takes account of the aerosol particles with larger diameters centering around 1.5 μ m, according to Eq. 3 and Fig. 8. Thus, the interception and impaction mechanisms play a more significant role in the filtration of these larger particles by the mask fabric if no leakage exists $^{9.33}$. Fig. 8 also displays that, due to relatively large Stokes numbers, these particles will have relatively small σ values and tend to penetrate the mask fabric instead of leaking via the mask periphery. Moreover, according to Darcy's law in Sec. II C 1, the increase of the air resistance C_k is associated with the increase (decrease) of the fiber density (fabric permeability). Therefore, when penetrating the mask fabric, these larger particles have a higher chance to impact or intercept with the fabric fibers and get filtered.

Taken together, an increase in air resistance C_k will cause a higher peripheral leakage ratio η (see Fig. 9a), subsequently reducing the total volume of filtered airflow. Yet, for the particle sizes considered by oFFE, most particles do not follow the airflow but try to penetrate the mask fabric. As a result, the rise in air resistance C_k will also result in the increase in the interception and impaction of particles by the mask fabric, ultimately leading to larger oFFE values.

5. FE_{min} at MPPS is often employed as the key defining metric for the face mask protection. However, Fig. 11c shows that nearly all types of mask fabrics in the present study provide oFFE greater than their corresponding FE_{min}. This finding indicates that with exhalation associated with normal breathing, FE_{min} is weakly correlated



PLEASE CITE THIS ARTICLE AS DOI: 10.1063/5.0153513

Accepted to Phys. Fluids 10.1063/5.0153513

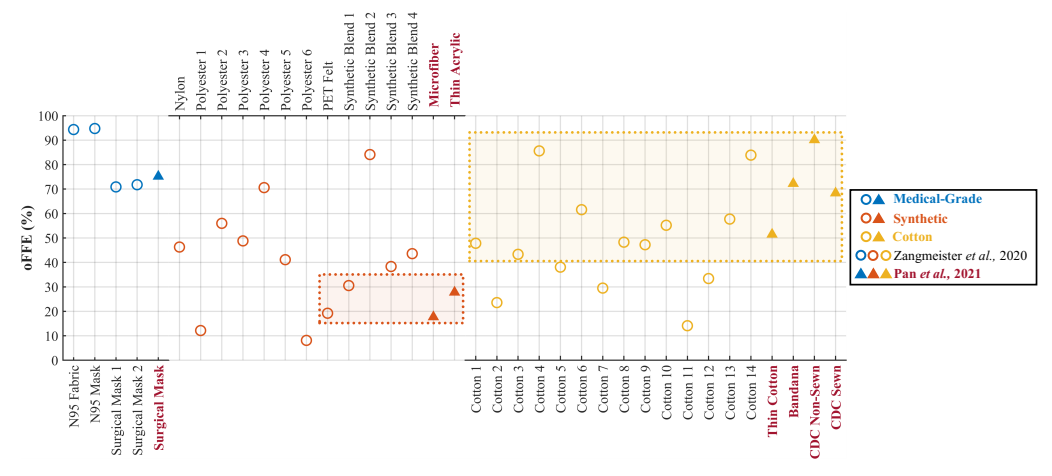


FIG. 12: **oFFE validation by fabrics in three categories:** oFFE of most of the fabrics included in the current study and in Pan *et al.*⁵⁴ are presented and classified into three general categories. Fabric names are listed in the x-axis, and they are consistent with the names used in Zangmeister *et al.*³² and in Pan *et al.*⁵⁴. The three categories are distinguished by the marker colors and are shown in the legend. Fabrics from different references are represented by different marker shapes (see the legend) and the fabrics from Pan *et al.*⁵⁴ are also highlighted in the fabric names by dark red color.

with oFFE and tends to underestimate, often significantly, the actual outward protection of face masks for filtering aerosol particles.

6. To sum up, these findings indicate that for normal breathing exhalation, all medical-grade masks and many cloth masks provide good to excellent filtration of the exhaled aerosol particles despite the significant peripheral leakage.

We now compare the predictions from the current model with available experimental data. Pan et al.54 employed mannequins with and without masks along with artificially generated aerosol particles to measure outward protection efficiency (OPE) as a function of particle diameter \overline{D} ranging from 0.5 to 5 μm with an exhalation jet velocity of 1.8 m/s. OPE is a ratio of the particles trapped by the mask to the total particles exhaled and is equivalent to $P_F(D)$ in Eq. 3. In the study of Pan et al.54 the masks were installed on a human mannequin and allowed to generate peripheral gaps naturally as a function of the stiffness of the mask material. Thus, they did not precisely control for or measure the size of the peripheral gaps, but we expect that the gaps from this procedure would be within the range explored by the current model. In other ways, the experimental conditions align well with those used in the current model and can be used for validating our oFFE predictions.

In order to conduct a consistent comparison with the oFFE from Eq. 3 in our model, curves are fitted to the discretized data point in Pan *et al.* 54 to form OPE(D) functions (see Fig. S3 in Supplementary Sec. S-III). Average oFFE for selected fabrics in their study are estimated by integrating this OPE(D) from 0.5 to 5 μ m with the same size distribution PDF $P_{\rm E}(D)$ utilized

in our model (see Fig. 8). Although one-to-one comparisons of oFFE between the two data sets are not possible since the fabrics are not precisely the same, we can make comparisons for three general categories: medical-grade masks, synthetic fabric masks, and cotton fabric masks.

13

Fig. 12 shows the results of the comparisons. oFFE for the surgical masks from the two studies agree very well with each other, with both showing a value of between 70% and 75%. Unfortunately, Pan *et al.*⁵⁴ did not measure OPE of N95 masks for us to include in the comparisons. For the synthetic fabric masks, only two data points can be obtained from Pan et al.'s measurements⁵⁴. Close to the range of these points, only two of our model predictions for synthetic fabric masks could be found (included in the orange box), and the other ten fabrics lie outside the range, showing great variation for this fabric category. For the last category of cotton fabric masks, oFFE for Pan et al.'s samples⁵⁴ lie between 50% and 90%, and the oFFE for nine out of fourteen cotton fabrics used in the current study lie in the range between 40% and 90% (included in the vellow box). For all the mask fabrics, data points from Pan et al. 54 mostly lie within the oFFE range estimated by the current model. Thus, in general, the agreement with the experiments is quite reasonable, especially considering the variability in the fabrics used as well as the uncertainties associated with both the experiments and our model.

Further assessment of our oFFE evaluations could be carried out by comparing to other studies. Driessche *et al.*⁵⁷ found out that surgical masks can filter out over 80% of *P. aeruginosa* infected aerosols generated by coughing in cystic fibrosis patients, and N95 masks perform better than surgical masks. Although the circumstances in this study do not match

PLEASE CITE THIS ARTICLE AS DOI: 10.1063/5.0153513

exactly to those in our model, in general, the outward protection evaluations of surgical and N95 masks align reasonably well with our oFFE predictions. Van der Sande, Teunis, and Sabel²⁹ also pointed out that the outward protection efficiency for surgical masks typically ranges from 50% to 70%, and Eikenberry et al.58 concluded that for typical outward protection efficiencies, homemade cloth masks may range from 0% to over 80% with an average around 50%, and for surgical and N95 masks these ranges are from 50% to 90% and from 70% to 100%, respectively. Moreover, by conducting dynamic flow simulations, Dbouk and Drikakis26 have found that the outward filtration efficiency of surgical masks can vary with time due to the cumulative effect of flow dynamics and the deterioration of the mask. After ten coughing cycles, oFFE of the surgical mask decreases from the initial value of 91% to the final value of 82%, which is quite close to our average oFFE predication around 70%. To sum up, all the above figures have a very reasonable agreement with our predictions of the face mask outward protection oFFE.

IV. DISCUSSION AND CONCLUSIONS

There is a significant body of scientific evidence demonstrating that community mask-wearing has been effective in reducing the spread of SARS-CoV-2^{59,60}. Numerous studies have shown that the use of masks in public settings significantly reduces the transmission of the virus by trapping the droplets expelled when people talk, cough, or sneeze. Studies in countries such as China⁶¹, Japan, and South Korea, where mask-wearing is a common practice, found that mask-wearing in the community reduces the spread of SARS-CoV-2.

How does this evidence reconcile with the fact that most face masks worn by people in a community setting allow peripheral leaks that would seemingly diminish their effectiveness? The current model and results provide a partial answer to this question. The results of the model show that despite large peripheral leakage (ranging upwards of 75% for most masks), face masks can filter out a significant fraction of exhaled aerosol particles. This is due to two primary factors: first, the vast majority of the exhaled particles do not follow the flow through the peripheral gaps, but instead, their inertia carries them into the face masks, where they are trapped by the mask fabrics as per their filtration efficiencies; and second, for the particle sizes involved in normal breathing, the filtration efficiencies of most masks are quite good.

Indeed, using the data from our model, we can attempt to estimate the effect of community mask-wearing considering the outward protection of face masks. Using the data for the nominal fit case, the average oFFE for N95 masks (2 samples), surgical masks (2 samples) and cloth masks (including cotton and synthetic fabrics, 26 samples) are approximately 95%, 72% and 45%, respectively. The type of mask worn by the public during the COVID-19 pandemic has depended on a variety of factors⁶²⁻⁶⁴, but surgical and cloth masks are by far the most common choices for face coverings. In Tab. I, we use these average oFFE with four different scenarios of mask-type preferences (M) among the public, to estimate the

TABLE I: Estimated rates of transmission reduction among the public due to inward and outward protection from face masks: four scenarios of face mask choices among the public are considered. The reduction rates due to the outward protection from face masks (R_{out}) are predicted based on the oFFE from the current model (see Eq. 9). To estimate the reduction rates provided by the combined effect of inward and outward protections ($R_{\text{out-in}}$), the measurements of inward FFE (iFFE) from Clapp *et al.*²⁴ are adopted and combined with the oFFE from the current model (see Eq. 11).

	Scenario	Mask-type preference (M)			Transmission reduction	
		Surgical	Cloth	N95	Rout	R _{out+in}
ſ	1	25%	75%	0%	52%	66%
ſ	2	50%	50%	0%	58%	72%
ĺ	3	75%	25%	0%	65%	77%
	4	33%	33%	33%	70%	87%

net reduction in airborne virus transmission (R_{out}). The percentage reduction in transmission is evaluated based on the following formula:

$$R_{\text{out}} = \left\{ 1 - \sum_{k=1}^{3} M_k \times (1 - \text{oFFE}_k) \right\} \times 100 \%,$$
 (9)

where M_k is the preference for the k^{th} mask type (M_1 : Surgical, M_2 : Cloth, or M_3 : N95), and oFFE_k is the outward FFE for the k^{th} mask type, with all these values expressed as fractional values (and not in percentage).

With the use of surgical and cloth masks alone (Scenarios 1 to 3), the outward filtration provided by normally worn face masks could reduce transmission rates by factors ranging from about 52% to 65%. In more recent times, N95 masks have become readily available and if we include these masks as options as well (Scenario 4), reduction in transmission rates due to outward protection alone could reach around 70%.

Airborne transmission of viruses ultimately depends on several factors. Indeed, according to Mittal, Meneveau, and Wu¹³. airborne transmission of viruses occurs when the Contagion Airborne Transmission (CAT) inequality is satisfied. CAT inequality is formulated as follows.

$$(\dot{R}_{h} \times n_{v} \times f_{mh}) \times (f_{ah} \times f_{at} \times f_{vv}) \times (f_{is} \times f_{ms} \times T_{s}) \ge N_{ID},$$
 (10)

where the symbols used above are explained in Tab. II.

As evident from the CAT inequality, the inward protection due to face masks (iFFE) provides a multiplicative effect ($f_{ms} \equiv 1$ -iFFE) that would further reduce the transmission rates. While our reduced-order mask model in its current form does not directly apply to the prediction of inward protection, we can estimate the transmission reduction considering both the outward and inward protections of face masks by combining our model's predictions for outward protection with available data for inward protection. For instance, Clapp et al.24 examined the inward FFE (iFFE) for a variety of masks via experiments and showed that for a typically worn 3-layer cotton mask, a surgical mask and an N95 mask, the iFFE are

PLEASE CITE THIS ARTICLE AS DOI: 10.1063/5.0153513

	rate of aerosol particle production from the nose and mouth of	Ì
$\dot{R}_{ m h}$	the infectious	l

R_h the infectious average number of virions contained in each exhaled aerosol

 $n_{\rm V}$ particles fraction of exhaled particles that make it past the face mask of $f_{\rm mh}$ the infectious (=1-oFFE)

fraction of exhaled particles that aerosolize (i.e., become sus f_{ah} pended in the air)

 f_{at} fraction of aerosolized particles transported to the vicinity of f_{at} the susceptible

fraction of aerosolized particles transported to the vicinity of

| f_{VV} the susceptible that contain viable virions | fraction of aerosol particles in the vicinity of the susceptible

 $f_{\rm is}$ that are inhaled by a susceptible not wearing a face mask fraction of inhaled aerosol particles that are not filtered by the

 f_{ms} face mask of the susceptible (=1-iFFE)

duration of exposure of the susceptible to the aerosol particles T_S from the infectious

minimum number of inhaled virions required to initiate infec- $N_{\rm ID}$ tion in the susceptible

about 27%, 39% and 98%, respectively. With these inward FFE data, Eq. 9 can be augmented to estimate the combined reduction in transmission ($R_{\text{out+in}}$) as follows:

$$R_{\text{out+in}} = \left\{ 1 - \sum_{k=1}^{3} M_k \times (1 - \text{oFFE}_k) \right. \\ \times \sum_{k=1}^{3} M_k \times (1 - \text{iFFE}_k) \right\} \times 100 \%,$$
 (11)

where iFFE $_k$ is the inward FFE for the k^{th} mask type, taken from the study of Clapp $et\ al.^{24}$. Estimates of R_{out+in} are also included in Tab. I, and overall, protection factors increase by 12% to 17% for the various scenarios when inward protection of face masks is included in addition to the outward protection. The inclusion of combined protections can therefore reduce the transmission rates from about 70% to nearly 90% for the mask-choice scenarios examined in this study. These estimates provide further support for policies that encourage widespread use of face masks for reducing the transmission of airborne diseases such as COVID-19. The model predictions also show that even simple cotton masks can be highly effective in reducing transmission rates.

Beyond the effect of outward and inward protections afforded by face masks, airborne transmission of viruses also depends on environmental factors such as relative humidity and temperature⁶⁵, the wind speed, and the distance between the infectious and the susceptible person¹³. These factors enter the CAT inequality (see Eq. 10) through one or more of the following variables: $f_{\rm ah}$, $f_{\rm at}$, and $f_{\rm vv}$. However, the ultimate influence of these factors on the transmission rate of virusladen aerosol particles remains difficult to quantify¹³, and is outside the scope of current study.

Evaluating the face mask outward protection based on particle counts is a widely used method and is reported in many

references ^{17,26,29,32,54,57,58}, and is the route chosen in the current study. The present model could however be extended to incorporate factors such as the particle volume and the viral load of particle (variable $n_{\rm V}$ in the CAT inequality (Eq. 10)) into the evaluation of face mask outward protection. To accomplish this task, the formula for oFFE should be modified into the following form:

offe =
$$\frac{\int_{D_0}^{D_1} \text{FE}(D) [1 - \sigma(\text{Stk})\eta] f_p(D) P_E(D) dD}{\int_{D_0}^{D_1} f_p(D) P_E(D) dD}, \quad (12)$$

where $f_{\rm p}(D)$ is a property function of particle at diameter D. For instance, $f_{\rm p}(D)$ could be the initial volume of a particle or the number of virions contained within it. In this way, the oFFE model can now be used to quantify the average particle volume or number of virions filtered by the mask. Accurate accounting for the particle volume and/or the number of virions in the particle is however a non-trivial task. First, large particles may break up into small particles when interacting with the airflow inside the mask or during the impact on the mask fabric. A breakup model, which is outside the scope of the present study, is then required to adjust the $f_{\rm p}(D)$ function for particle breakups. Second, the viral load may also vary over a wide range $(10^2-10^7$ RNA copies/mL) due to many factors (e.g., age, infection severity and time, etc.) $^{66.67}$ which are difficulty to account for.

We note in closing that the model is currently limited to normal breathing and does not apply to exhalation events such as coughing and sneezing, nor to inhalation. The model could however, in principle, be extended to include these conditions. The current face mask model also does not consider the spatial variations in pressure in the flow volume inside the mask, and we speculate that regional variations in pressure within this region could modify (most likely reduce) the leakage fluxes. Regional variations of pressure could be included via inviscid models, or by incorporating data from viscous flow simulations, but these would increase the complexity of the model. Given that the flow inside the mask is expected to have a temperature and humidity similar to those in the nasal cavity, particle evaporation effects are not expected to be significant to include in the current model. The model also does not account for the rebound or breakup of exhaled aerosol particles due to their interaction with both the airflow and mask fabrics⁹. As indicated by Dbouk and Drikakis26, these exhaled particlesespecially those with larger diameters-may break up when interacting with the airflow and fabric fibers, and potentially rebound upon impacting the mask fabrics. Such factors could lead to an increased number of smaller particles escaping from the peripheral gaps and penetrating the mask fabrics, thereby diminishing the outward protection of face masks. However, these complex interactions are outside the scope of the current model and have uncertainties to be further explored. Thus, despite these limitations, we have shown that the model can serve as a useful tool for assessing the outward protection afforded by face masks. The model has also added further evidence for why simple cloth masks, even when worn without being fitted tightly to the face, have been effective in reducing the transmission rates of SARS-CoV-2^{4,5,59-61}

This is the author's peer reviewed, accepted manuscript. However, the online version of record will be different from this version once it has been copyedited and typeset PLEASE CITE THIS ARTICLE AS DOI: 10.1063/5.0153513

Accepted to Phys. Fluids 10.1063/5.0153513

SUPPLEMENTARY MATERIAL

See supplementary material for the validation of filtration efficiency (FE) extrapolation in Sec. S-I, the experimental data of investigated mask fabrics in Sec. S-II, and the curves of outward protection efficiency (OPE) from Pan *et al.* ⁵⁴ in Sec. S-III.

ACKNOWLEDGMENTS

This work was supported by National Science Foundation Grants CBET-2034983 and CBET-2034992.

AUTHOR DECLARATIONS

Conflict of Interest

The authors have no conflicts to disclose.

DATA AVAILABILITY STATEMENT

The data that support the findings of this study are available from the corresponding author upon reasonable request.

REFERENCES

- ¹CDC, "Masks and Respirators," https://www.cdc.gov/coronavirus/2019ncov/prevent-getting-sick/about-face-coverings.html (2022).
- ²WHO, "When and how to use masks," https://www.who.int/emergencies/diseases/novel-coronavirus-2019/advice-for-public/when-and-how-to-use-masks (2021).
- 3Z. Zhai, "Facial mask: A necessity to beat COVID-19," Build Environ 175, 106827 (2020).
- ⁴Y. Li, M. Liang, L. Gao, M. Ayaz Ahmed, J. P. Uy, C. Cheng, Q. Zhou, and C. Sun, "Face masks to prevent transmission of COVID-19: A systematic review and meta-analysis," American Journal of Infection Control 49, 900– 906 (2021).
- 58. Feng, C. Shen, N. Xia, W. Song, M. Fan, and B. J. Cowling, "Rational use of face masks in the COVID-19 pandemic," The Lancet Respiratory Medicine 8, 434–436 (2020).
- ⁶Y. Chen, X. Tong, J. Wang, W. Huang, S. Yin, R. Huang, H. Yang, Y. Chen, A. Huang, Y. Liu, Y. Chen, L. Yuan, X. Yan, H. Shen, and C. Wı, "High SARS-CoV-2 antibody prevalence among healthcare workers exposed to COVID-19 patients," Journal of Infection 81, 420–426 (2020).
- ⁷P. Doung-ngern, R. Suphanchaimat, A. Panjangampatthana, C. Janekrongtham, D. Ruampoom, N. Daochaeng, N. Eungkanit, N. Pisitpayat, N. Srisong, O. Yasopa, P. Plernprom, P. Promduangsi, P. Kumphon, P. Suangtho, P. Watakulsin, S. Chaiya, S. Kripattanapong, T. Chantian, E. Bloss, C. Namwat, and D. Limmathurotsakul, "Case-Control Study of Use of Personal Protective Measures and Risk for SARS-CoV 2 Infection, Thailand," Emerg Infect Dis 26, 2607–2616 (2020).
- ⁸A. Heinzerling, M. J. Stuckey, T. Scheuer, K. Xu, K. M. Perkins, H. Resseger, S. Magill, J. R. Verani, S. Jain, M. Acosta, and E. Epson, "Transmission of COVID-19 to Health Care Personnel During Exposures to a Hospitalized Patient Solano County, California, February 2020," MMWR Morb Mortal Wkly Rep 69, 472–476 (2020).
- ⁹R. Mittal, K. Breuer, and J. H. Seo, "The Flow Physics of Face Masks," Annual Review of Fluid Mechanics 55, 193–211 (2023).

¹⁰K. P. Fennelly, "Particle sizes of infectious aerosols: Implications for infection control," The Lancet Respiratory Medicine 8, 914–924 (2020).

16

- ¹¹C. C. Wang, K. A. Prather, J. Sznitman, J. L. Jimenez, S. S. Lakdawala, Z. Tufekci, and L. C. Marr, "Airborne transmission of respiratory viruses," Science 373, eabd9149 (2021).
- ¹²R. Mittal, R. Ni, and J.-H. Seo, "The flow physics of COVID-19," Journal of Fluid Mechanics 894, F2 (2020).
- ¹³R. Mittal, C. Meneveau, and W. Wu, "A mathematical framework for estimating risk of airborne transmission of COVID-19 with application to fore most use and social distancing," Physics of Fluids 32, 101903 (2020).
- face mask use and social distancing," Physics of Fluids 32, 101903 (2020).

 ¹⁴Y. Bai, L. Yao, T. Wei, F. Tian, D.-Y. Jin, L. Chen, and M. Wang, "Presumed Asymptomatic Carrier Transmission of COVID-19," JAMA 323, 1406–1407 (2020).
- ¹⁵D. S. Hui, B. K. Chow, L. Chu, S. S. Ng, N. Lee, T. Gin, and M. T. V. Chan, "Exhaled Air Dispersion during Coughing with and without Wearing a Surgical or N95 Mask," PLOS ONE 7, e50845 (2012).
 ¹⁶S. Verma, M. Dhanak, and J. Frankenfield, "Visualizing the effectiveness
- ¹⁶S. Verma, M. Dhanak, and J. Frankenfield, "Visualizing the effectiveness of face masks in obstructing respiratory jets," Physics of Fluids 32, 061708 (2020).
- ¹⁷E. Drewnick, J. Pikmann, F. Fachinger, L. Moormann, F. Sprang, and S. Bormann, "Aerosol filtration efficiency of household materials for homemade face masks: Influence of material properties, particle size, particle electrical charge, face velocity, and leaks," Aerosol Science and Technology 55, 63–79 (2021).
- ¹⁸J. W. Tang, T. J. Liebner, B. A. Craven, and G. S. Settles, "A schlieren optical study of the human cough with and without wearing masks for aerosol infection control," Journal of The Royal Society Interface 6, S727–S736 (2009).
- 3/30 (2007).
 19 D. Lepelletier, B. Grandbastien, S. Romano-Bertrand, S. Aho, C. Chidiac, J. F. Géhanno, and F. Chauvin, "What face mask for what use in the context of the COVID-19 pandemic? The French guidelines," Journal of Hospital Infection 105, 414–418 (2020).
- 20 S. Das, S. Sarkar, A. Das, S. Das, P. Chakraborty, and J. Sarkar, "A comprehensive review of various categories of face masks resistant to Covid-19," Clinical Epidemiology and Global Health 12, 100835 (2021).
- T. J. Ju, L. N. Boisvert, and Y. Y. Zuo, "Face masks against COVID-19: Standards, efficacy, testing and decontamination methods," Advances in Colloid and Interface Science 292, 102435 (2021).
- ²²L. H. Kwong, R. Wilson, S. Kumar, Y. S. Crider, Y. Reyes Sanchez, D. Rempel, and A. Pillarisetti, "Review of the Breathability and Filtration Efficiency of Common Household Materials for Face Masks," ACS Nano 15, 5904—5924 (2021).
- ²³ X. Mao and A. E. Hosoi, "Estimating the filtration efficacy of cloth masks," Phys. Rev. Fluids 6, 114201 (2021).
- ²⁴P. W. Clapp, E. E. Sickbert-Bennett, J. M. Samet, J. Berntsen, K. L. Zeman, D. J. Anderson, D. J. Weber, W. D. Bennett, and US Centers for Disease Control and Prevention Epicenters Program, "Evaluation of Cloth Masks and Modified Procedure Masks as Personal Protective Equipment for the Public During the COVID-19 Pandemic," JAMA Internal Medicine 181, 463–469 (2021).
- ²⁵Z. Lei, J. Yang, Z. Zhuang, and R. Roberge, "Simulation and Evaluation of Respirator Faceseal Leaks Using Computational Fluid Dynamics and Infrared Imaging," The Annals of Occupational Hygiene 57, 493–506 (2013).
- ²⁶T. Dbouk and D. Drikakis, "On respiratory droplets and face masks," Physics of Fluids 32, 063303 (2020).
- ²⁷T. Solano, C. Ni, R. Mittal, and K. Shoele, "Perimeter leakage of face masks and its effect on the mask's efficacy," Physics of Fluids 34, 051902 (2022).
- ²⁸TIMO. TUOMI, "Face Seal Leakage of Half Masks and Surgical Masks," American Industrial Hygiene Association Journal 46, 308–312 (1985).
- ²⁹M. Van der Sande, P. Teunis, and R. Sabel, "Professional and Home-Made Face Masks Reduce Exposure to Respiratory Infections among the General Population," PLOS ONE 3, e2618 (2008).
- ³⁰ W. C. Hill, M. S. Hull, and R. I. MacCuspie, "Testing of Commercial Masks and Respirators and Cotton Mask Insert Materials using SARS-CoV-2 Virion-Sized Particulates: Comparison of Ideal Aerosol Filtration Efficiency versus Fitted Filtration Efficiency," Nano Lett. 20, 7642–7647 (2020).
- ³¹G. Bagheri, B. Thiede, B. Hejazi, O. Schlenczek, and E. Bodenschatz, "An upper bound on one-to-one exposure to infectious human respiratory particles," Proceedings of the National Academy of Sciences 118, e2110117118

PLEASE CITE THIS ARTICLE AS DOI: 10.1063/5.0153513

Accepted to Phys. Fluids 10.1063/5.0153513

(2021).

- ³²C. D. Zangmeister, J. G. Radney, E. P. Vicenzi, and J. L. Weaver, "Filtration Efficiencies of Nanoscale Aerosol by Cloth Mask Materials Used to Slow the Spread of SARS-CoV-2," ACS Nano 14, 9188–9200 (2020).

 ³³D. Thomas, A. Charvet, N. Bardin-Monnier, and J.-C. Appert-Collin,
- Aerosol Filtration (Elsevier, 2016).
- Aerob. Filmann (Liscov., 2016), ⁴Y. M. Bar-On, A. Flamholz, R. Phillips, and R. Milo, "SARS-CoV-2 (COVID-19) by the numbers," eLife **9**, e57309 (2020).
- ³⁵G. R. Johnson, L. Morawska, Z. D. Ristovski, M. Hargreaves, K. Mengersen, C. Y. H. Chao, M. P. Wan, Y. Li, X. Xie, D. Katoshevski, and S. Corbett, "Modality of human expired aerosol size distributions," Journal of Aerosol Science 42, 839–851 (2011).
- ³⁶W. C. Hinds and Y. Zhu, Aerosol Technology: Properties, Behavior, and Measurement of Airborne Particles (John Wiley & Sons, 2022)
- ³⁷K. W. Lee and B. Y. H. Liu, "Theoretical Study of Aerosol Filtration by Fibrous Filters," Aerosol Science and Technology 1, 147-161 (1982).
- ³⁸R. Perić and M. Perić, "Analytical and Numerical Investigation of the Airflow in Face Masks used for Protection against COVID-19 Virus -Implications for Mask Design and Usage," Journal of Applied Fluid Mechanics 13, 1911-1923 (2020).
- ³⁹C. Y. H. Chao, M. P. Wan, L. Morawska, G. R. Johnson, Z. D. Ristovski, M. Hargreaves, K. Mengersen, S. Corbett, Y. Li, X. Xie, and D. Katoshevski, "Characterization of expiration air jets and droplet size distributions immediately at the mouth opening," Journal of Aerosol Science 40, 122–133
- Addison Portion (Control of Pluids in Porous Media (Courier Corporation, 2013).
 Al O. Aydin, B. Emon, S. Cheng, L. Hong, L. P. Chamorro, and M. T. A. Saif, "Performance of fabrics for home-made masks against the spread of COVID-19 through droplets: A quantitative mechanistic study," Extreme Mechanics Letters **40**, 100924 (2020).
- 42 S.-B. Kwon, J. Park, J. Jang, Y. Cho, D.-S. Park, C. Kim, G.-N. Bae, and A. Jang, "Study on the initial velocity distribution of exhaled air from
- coughing and speaking," Chemosphere 87, 1260–1264 (2012). ⁴³W. Du, F. Iacoviello, T. Fernandez, R. Loureiro, D. J. L. Brett, P. R. Shearing, "Microstructure analysis and image-based modelling of face
- masks for COVID-19 virus protection," Commun Mater 2, 1–10 (2021). ⁴⁴T. Solano, R. Mittal, and K. Shoele, "One size fits all?: A simulation framework for face-mask fit on population-based faces," PLOS ONE 16, e0252143 (2021).
- ⁴⁵J. Schmitt and J. Wang, "A critical review on the role of leakages in the facemask protection against SARS-CoV-2 infection with consideration of vaccination and virus variants," Indoor Air 32, e13127 (2022).
- ⁴⁶P. Bourrianne, N. Xue, J. Nunes, M. Abkarian, and H. A. Stone, fying the effect of a mask on expiratory flows," Phys. Rev. Fluids 6, 110511
- ⁴⁷J. Xi, K. Barari, X. A. Si, M. Y. Abdollahzadeh Jamalabadi, J. H. Park, and M. Rein, "Inspiratory leakage flow fraction for surgical masks with varying gaps and filter materials," Physics of Fluids 34, 041908 (2022).

 48 H. Jung, J. K. Kim, S. Lee, J. Lee, J. Kim, P. Tsai, and C. Yoon, "Comparison
- of Filtration Efficiency and Pressure Drop in Anti-Yellow Sand Masks, Quarantine Masks, Medical Masks, General Masks, and Handkerchiefs," Aerosol Air Qual. Res. 14, 991-1002 (2014).
- ⁴⁹R. M. Eninger, T. Honda, A. Adhikari, H. Heinonen-Tanski, T. Reponen, and S. A. Grinshpun, "Filter Performance of N99 and N95 Facepiece Respirators Against Viruses and Ultrafine Particles," The Annals of Occupational Hygiene 52, 385-396 (2008).
- ⁵⁰ Y. S. Cheng and C. S. Wang, "Motion of particles in bends of circular pipes," Atmospheric Environment (1967) 15, 301-306 (1981).

51D, Y. H. Pui, F. Romay-Novas, and B. Y. H. Liu, "Experimental Study of Particle Deposition in Bends of Circular Cross Section," Aerosol Science and Technology 7, 301-315 (1987).

17

- ⁵²V. A. Schriever, T. Hummel, J. N. Lundström, and J. Freiherr, "Size of nostril opening as a measure of intranasal volume," Physiology & Behavior
- ⁵³N. L. Phuong and K. Ito, "Investigation of flow pattern in upper human airway including oral and nasal inhalation by PIV and CFD," Building and Environment 94, 504-515 (2015).
- ⁵⁴J. Pan, C. Harb, W. Leng, and L. C. Marr, "Inward and outward effectiveness of cloth masks, a surgical mask, and a face shield," Aerosol Science and Technology 55, 718-733 (2021).
- ⁵⁵P. S. Larsen, J. Heebøll, and K. E. Meyer, "Measured Air Flow Leakage in Facemask Usage," International Journal of Environmental Research and Public Health 20, 2363 (2023).
- ⁵⁶S. Freitag, S. G. Howell, and K. T. C. Jim, "Estimating the reduction in SARS-CoV-2 viral load by common face masks with a simple leak model,' Aerosol Science and Technology 56, 573–591 (2022).
- ⁵⁷ K. V. Driessche, N. Hens, P. Tilley, B. S. Quon, M. A. Chilvers, R. de Groot, M. F. Cotton, B. J. Marais, D. P. Speert, and J. E. A. Zlosnik, "Surgical Masks Reduce Airborne Spread of Pseudomonas aeruginosa in Colonized Patients with Cystic Fibrosis," Am J Respir Crit Care Med 192, 897-899
- ⁵⁸S. E. Eikenberry, M. Mancuso, E. Iboi, T. Phan, K. Eikenberry, Y. Kuang, E. Kostelich, and A. B. Gumel, "To mask or not to mask: Modeling the potential for face mask use by the general public to curtail the COVID-19
- pandemic," Infect Dis Model S, 293–308 (2020).

 ⁵⁹J. T. Brooks, J. C. Butler, and R. R. Redfield, "Universal Masking to Prevent SARS-CoV-2 Transmission—The Time Is Now," JAMA 324, 635-
- 60 N. H. L. Leung, D. K. W. Chu, E. Y. C. Shiu, K.-H. Chan, J. J. McDevitt, B. J. P. Hau, H.-L. Yen, Y. Li, D. K. M. Ip, J. S. M. Peiris, W.-H. Seto, G. M. Leung, D. K. Milton, and B. J. Cowling, "Respiratory virus shedding in exhaled breath and efficacy of face masks," Nat Med **26**, 676–680 (2020).
- ⁶¹ Y. Wang, H. Tian, L. Zhang, M. Zhang, D. Guo, W. Wu, X. Zhang, G. L. Kan, L. Jia, D. Huo, B. Liu, X. Wang, Y. Sun, Q. Wang, P. Yang, and C. R. MacIntyre, "Reduction of secondary transmission of SARS-CoV-2 in households by face mask use, disinfection and social distancing: A cohort study in Beijing, China," BMJ Global Health 5, e002794 (2020).
- ⁶²L. Matusiak, M. Szepietowska, P. K. Krajewski, R. Białynicki-Birula, and J. C. Szepietowski, "The use of face masks during the COVID-19 pandemic in Poland: A survey study of 2315 young adults," Dermatol Ther 33, e13909
- 63L. C. Barrios, "Observed Face Mask Use at Six Universities United States, September–November 2020," MMWR Morb Mortal Wkly Rep 70 (2021), 10.15585/mmwr.mm7006e1.
- ⁶⁴K. Selvaranjan, S. Navaratnam, P. Rajeev, and N. Ravintherakumaran, "Environmental challenges induced by extensive use of face masks during COVID-19: A review and potential solutions," Environmental Challenges 3, 100039 (2021).
- 65T. Dbouk and D. Drikakis, "Weather impact on airborne coronavirus survival," Physics of Fluids 32, 093312 (2020).
- 65S. Anand and Y. S. Mayya, "Size distribution of virus laden droplets from expiratory ejecta of infected subjects," Sci Rep 10, 21174 (2020).
- ⁶⁷S, Zheng, J. Fan, F. Yu, B. Feng, B. Lou, Q. Zou, G. Xie, S. Lin, R. Wang, X. Yang, W. Chen, Q. Wang, D. Zhang, Y. Liu, R. Gong, Z. Ma, S. Lu, Y. Xiao, Y. Gu, J. Zhang, H. Yao, K. Xu, X. Lu, G. Wei, J. Zhou, Q. Fang, H. Cai, Y. Qiu, J. Sheng, Y. Chen, and T. Liang, "Viral load dynamics and disease severity in patients infected with SARS-CoV-2 in Zhejiang province, China, January-March 2020: Retrospective cohort study," BMJ 369, m1443